Bendola Publishing
Journal of Transition Metal Complexes
Vol. 2 (2019), Article ID 236083, 11 pages
doi:10.32371/jtmc/236083

Research Article

Structure, Optical, and Magnetic Properties of Magnetite Nanoparticles Doped with Zinc and Lanthanum and Prepared in Oxygen and Nitrogen Atmosphere

D. A. Rayan,[1] M. A. Zayed,[2] and G. M. Abd Al Maqsoud[2]

[1] *Central Metallurgical Research and Development Institute (CMRDI), Helwan, 11421 Cairo, Egypt*
[2] *Chemistry Department, Faculty of Science, University of Cairo, 12613 Giza, Egypt*
Address correspondence to G. M. Abd Al Maqsoud, chemgehad200@yahoo.com

Received 9 November 2019; Revised 22 December 2019; Accepted 23 December 2019

Abstract A comparative study of structural and magnetic properties for the Zn^{2+} and La^{3+} ions co-doped magnetite nanoparticles of the general formula [(1-x)Fe_3O_4:Zn:xLa, where $x = 0.0$, 0.1, 0.15, 0.2, 0.25, and 0.3] was prepared via co-precipitation method under oxygen and nitrogen atmosphere. The stoichiometric ratios of the elements in the given general formula were proved and confirmed by both Inductively coupled plasma (ICP) measurements and atomic absorption data. Various analytical and characterization techniques were used to analyze the prepared nanoparticles. X-ray diffraction (XRD) confirmed the formation of one single phase of nanoparticles components with average crystalline size ranging from 6.0 nm to 9.0 nm at oxygen atmosphere and from 6.0 nm to 8.0 nm at nitrogen atmosphere. These size values were calculated by Debye-Scherrer equation. The morphology of Zn^{2+} and La^{3+} ions co-doped magnetite nanoparticles was studied using field-emission scanning electron microscope (FE-SEM) and high-resolution transmission electron microscope (HR-TEM). Optical properties were demonstrated by UV-visible-NIR spectrophotometer. The high absorbance values of $ZnLa_{(x)}Fe_{(3-x)}O_4$ were found to be 80–97% and 80–99% in the visible wavelength range of 400–800 nm for the prepared samples in the presence of O_2 and N_2 gases at room temperature, respectively; which proved the lower values of energy bandgap in both conditions. The lowering of energy bandgap of 1.89 eV for nanoparticles prepared in O_2 gas and 1.78 eV for those prepared in N_2 gas in most samples may be attributed to incorporation of Zn cation. Magnetic properties of the given samples, obtained from vibrating sample magnetometer (VSM), showed that most of these samples exhibited almost superparamagnetic behavior. These magnetic values (32.87 emu/g and 24.79 emu/g) infer super saturation magnetization of the given samples prepared in O_2 and N_2 gases at room temperature, respectively. Examination of the magnetic properties revealed decrease in saturation magnetization with increasing La ion concentrations incorporation up to $x = 0.3$.

Keywords magnetite; nanoparticles; co-precipitation; Zn and La doping; optical and magnetic properties

1. Introduction

Iron oxide nanoparticles (IONPs) include many attributes of high magnetic saturation, stability, biocompatibility, and interactive functions at the surface [1]. The surface of IONPs could be adjusted by organic materials or inorganic materials, such as polymers, biomolecules, silica, metals, and others, that improve from its properties [2]. The synthesis of magnetic IONPs has been greatly developed not only for its fundamental scientific interest but also for its many technological applications, such as targeted drug delivery, magnetic resonance imaging (MRI), magnetic hyperthermia and thermoablation, bioseparation, and biosensing [3,4]. Besides, bioapplications based on magnetic nanoparticles offer unique advantages over other materials such as being inexpensive to produce, physically and chemically stable, biocompatible, and environmentally safe [5]. IONPs have a large surface area and can be engineered to provide a large number of functional groups for cross-linking to tumor-targeting ligands such as monoclonal antibodies, peptides, or small molecules for diagnostic imaging or the delivery of therapeutic agents [6].

In the last few decades, the synthesis of magnetite (Fe_3O_4) and maghemite (γ-Fe_2O_3) using hematite (α-Fe_2O_3) as a starting material has been intensively pursued for both their fundamental scientific interests and technological applications [7]. Magnetite (Fe_3O_4) has the face-centered cubic spinel structure, based on 32 O^{2-} ions, and close-packed along the direction [8]. Fe_3O_4 differs from most other iron oxides in that it contains both divalent and trivalent iron. Fe_3O_4 has a cubic inverse spinel structure that consists of a cubic close-packed array of oxide ions, where all of the Fe^{2+} ions occupy half of the octahedral sites and the Fe^{3+} ions are split evenly across the remaining octahedral sites and the tetrahedral sites. In stoichiometric magnetite $Fe^{2+}/Fe^{3+} = 1/2$, and the divalent irons may be partly or fully replaced by other divalent ions (Co, Mn, Zn, etc.). Thus, Fe_3O_4 can be both an n- and p-type semiconductor; while it has the lowest resistivity among iron oxides due to its small bandgap (0.1 eV) [9].

A variety of synthetic methods such as co-precipitation [10], thermal decomposition [11], hydrothermal and

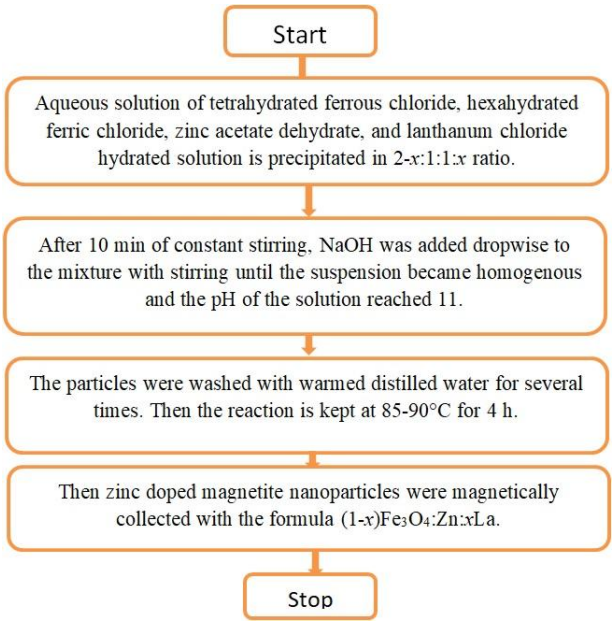

Scheme 1: Schematic diagram for the preparation of Zn-La doped magnetite nanoparticle.

solvothermal syntheses, sol-gel synthesis [12], microemulsion, ultrasound irradiation, and biological synthesis have been applied to produce magnetic IONPs [13]. As the most conventional method, the co-precipitation method consists of mixing ferric and ferrous ions in a 1:2 molar ratio in very basic solutions at room temperature or at elevated temperature. The reaction mechanism can be simplified as

$$\mathrm{Fe^{2+} + 2\,Fe^{3+} + 8\,OH^- \leftrightarrows Fe(OH)_2 + 2\,Fe(OH)_3} \rightarrow \mathrm{Fe_3O_4 \downarrow + 4\,H_2O.}$$

The ferric nanoparticles were coated with sheets of ferrous to produce magnetite nanoparticles [14].

After many research works, it has been proved that the magnetite nanoparticles can be improved further by doping [15]. The synthesis of magnetite in the presence of divalent and trivalent cations of transition metals (viz V^{3+}, Zn^{2+}, Cr^{3+}, Mn^{2+}, Co^{2+}, Ni^{2+}, and Li^{2+}) can modify electrical, magnetic, structural, optical, and saturation magnetization properties of iron oxide; these properties are helpful in understanding the mechanism of formation of rust in alloy elements and also help to better understand the factors which influence magnetism change because of impurities [12, 14].

In this study, we describe the careful investigation of Zn^{2+} and La^{3+} ions co-doped magnetite nanostructures upon their change in phase structure, crystallite sizes, space lattice parameters, and crystal morphologies. Moreover, the improvement in the optical properties of the prepared samples using UV-Vis-NIR was studied. The ultraviolet-visible spectroscopy was carried out in order to inspect optical reflectivity and also clarify the bandgap energy characteristics of the produced materials. The magnetic properties of the prepared materials were determined by means of the magnetic susceptibility and vibrating sample magnetometer (VSM).

2. Experimental

2.1. Materials and reagents

Tetrahydrate ferrous chloride $FeCl_2 \cdot 4\,H_2O$ (M.wt = 198.81 g mol^{-1}) was purchased from Research-Lab Fine Chem Industries (Maharashtra, India). Zinc acetate dihydrate $Zn(CH_3COO)_2 \cdot 2\,H_2O$ (M.wt = 219.50 g) was purchased from Oxford Lab Fine Chem (Maharashtra, India). Hexahydrate ferric chloride $FeCl_3 \cdot 6\,H_2O$ (M.wt = 270.30 g mol^{-1}), sodium hydroxide NaOH (M.wt = 40 g mol^{-1}), and lanthanum chloride $LaCl_3 \cdot 7\,H_2O$ (M.wt = 371.37 g mol^{-1}) were purchased from Alpha Chemika (Maharashtra, India). Hydrochloric acid (HCl) (M.wt = 36.46 g mol^{-1}) with purity 30–34% was purchased from Adwic (Qaliubiya, Egypt) and ethyl alcohol (ethanol) (M.wt = 46.07 g mol^{-1}) was purchased from International Company for SUP and MED Industries (Giza, Egypt). The distilled water used in all preparations is usually collected from all glass equipment. All chemicals used were of analytic grade.

2.2. Preparation of lanthanum and zinc doped magnetite nanoparticles

Aqueous solution of tetrahydrate ferrous chloride (0.4 M), zinc acetate dihydrate (0.2 M), and hexahydrate ferric chloride (0.2 M) was added in 2:1:1 ratio and the same volumes were taken from each solution (50 mL). After 10 min of constant stirring, NaOH was added drop-wise to the mixture with stirring until the suspension became homogenous and the pH of the solution reached 11; that was in the presence of oxygen atmosphere (O_2) once and then repeated again in the presence of nitrogen atmosphere, where (N_2) gas flow (with 99.9% of purity) continued for 20 min. The particles were washed with warmed distilled water several times [16]. Then the reaction was kept at 85–90 °C for 4 h. Afterwards, zinc doped magnetite nanoparticles were magnetically collected with the formula $ZnFe_3O_4$.

Then, the aqueous solutions of tetrahydrate ferrous chloride, zinc acetate dihydrate, and hexahydrate ferric chloride were mixed by 50 mL of the aqueous solution of lanthanum chloride $7 \cdot H_2O$ for different ratios (0.1, 0.15, 0.2, 0.25, and 0.3 M). Also after 10 min of constant stirring, NaOH was added drop-wise to the mixture with stirring until the suspension became homogenous and the pH of the solution reached 11. The reactions occured in the presence of oxygen and then in a nitrogen atmosphere. The particles were washed with warmed distilled water several times. The reaction was kept at 85–90 °C for 4 h. Then Zn-La doped

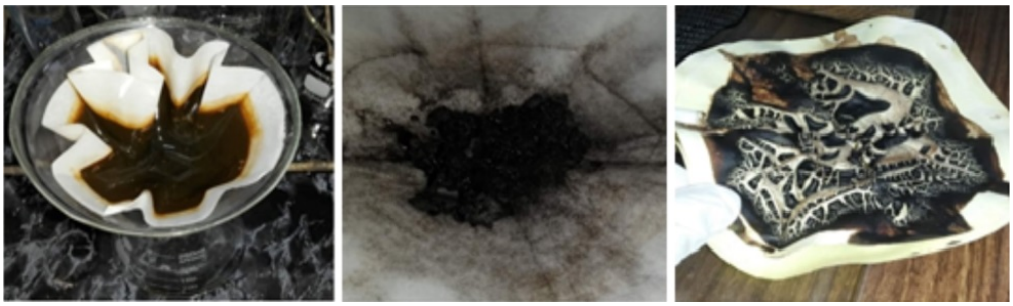

Figure 1: Images during preparation of Zn-La magnetite nanoparticles.

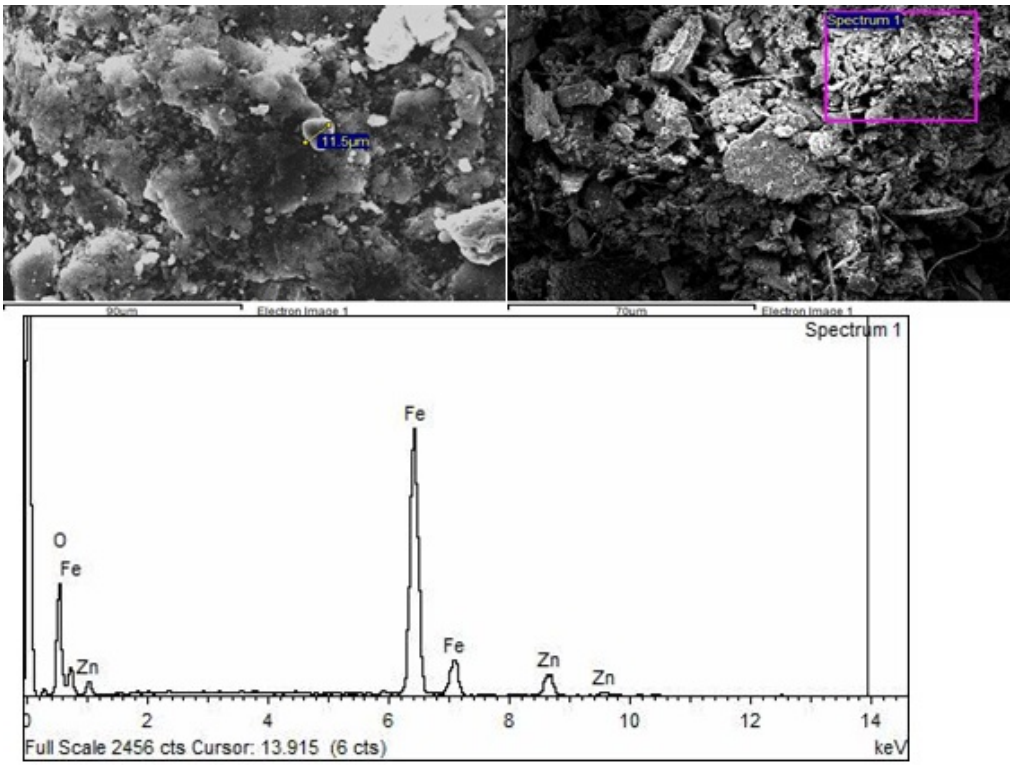

Figure 2: EDX results for sample (1-x)Fe_3O_4:Zn:xLa, where $x = 0.0$ at O_2 atmosphere.

magnetite nanoparticles were magnetically collected having the proposed formula [(1-x)Fe_3O_4:Zn:xLa, where x = 0.0, 0.1, 0.15, 0.2, 0.25, and 0.3]. The collected precipitates are shown in Figure 1, which were obtained by following Scheme 1 of precipitation.

2.3. Analytical characterization: chemical compositions

Different techniques were used to ensure that the phase in the nanocomposites was continued to (1-x)Fe_3O_4:Zn:xLa and to confirm the formation of a single-phase structure.

2.3.1. Energy-dispersive X-ray spectroscopy (EDX)

Table 1 shows that the main components of the sample are iron, zinc, and oxygen, which describes the presence of iron oxide and zinc oxide. The spectrum in Figure 2 contained three peaks which refer to Fe, Zn, and O; there are no other impurities identified.

2.3.2. Atomic absorption and ICP

Tables 2, 3, and 4 show the atomic absorption and ICP rates for the three elements, iron, zinc, and lanthanum used in the preparation of Zn-La magnetite nanoparticles.

2.4. Characterization

X-ray diffraction (XRD) patterns of the resulting products were characterized by a Brucker D8-advanced X-ray powder diffractometer with Cu Kα radiation (λ = 1.5406 Å). The crystallite sizes of the produced Zn^{2+} and La^{3+} ions co-doped magnetite nanostructures for the most intense peak

Table 1: The percentages of iron, zinc, and oxygen obtained from EDX analysis for the sample (1-x)Fe_3O_4:Zn:xLa, where $x = 0.0$ at O_2 atmosphere.

Element	Weight (%)	Atomic (%)
O K	38.90	69.45
Fe K	51.64	26.41
Zn K	9.46	4.13
Total	100.00	

Table 2: The iron used for the preparation of Zn-La magnetite nanoparticles.

X ratio	Fe % TH	Fe % AAS	Fe % ICP
0.0 O_2	58.1	52.99	
0.0 N_2	58.1	40.21	
0.1 O_2	39.48	37.9	40.92
0.1 N_2	39.48	37.68	42.6
0.15 O_2	37.64	35.17	25.92
0.15 N_2	37.64	39.5	31.98
0.2 O_2	35.9	38.65	41.52
0.2 N_2	35.9	37.57	37.5
0.25 O_2	34.26	30.42	40.32
0.25 N_2	34.26	31.38	38.34
0.3 O_2	32.7	38.55	31.68
0.3 N_2	32.7	33.44	37.92

Table 3: The zinc used for the preparation of Zn-La magnetite nanoparticles.

X ratio	Zn % TH	Zn % AAS	Zn % ICP
0.0 O_2	16.99	13.53	
0.0 N_2	16.99	8.21	
0.1 O_2	15.93	7.43	15.54
0.1 N_2	15.93	7.5	15.94
0.15 O_2	15.46	2.77	9.7
0.15 N_2	15.46	4.02	16.48
0.2 O_2	15	3.95	15.82
0.2 N_2	15	3.98	12.72
0.25 O_2	14.59	3.76	18.48
0.25 N_2	14.59	3.56	8.58
0.3 O_2	14.18	3.84	14.1
0.3 N_2	14.18	6.52	9.22

(3 1 1) plane were determined from the X-ray diffraction data using the Debye-Scherrer equation as follows [17]:

$$d_{RX} = k\lambda/\beta\cos\theta, \quad (1)$$

where d_{RX} is the crystallite size, $k = 0.9$ is a correction factor to account for particle shapes, β is the full width at half maximum (FWHM) of the most intense diffraction peak (3 1 1) plane, λ is the wavelength of Cu target = 1.5406 Å, and θ is the Bragg angle.

The micrographs of produced samples were examined by direct observation via FE-SEM model JEOL instrument (Japan) model JSM-7800F.

Table 4: The lanthanum used for the preparation of Zn-La magnetite nanoparticles.

X ratio	La % TH	La % ICP
0.0 O_2	0	
0.0 N_2	0	
0.1 O_2	3.38	2.66
0.1 N_2	3.38	2.9
0.15 O_2	4.9	2.38
0.15 N_2	4.9	4.72
0.2 O_2	6.4	6.02
0.2 N_2	6.4	6.28
0.25 O_2	7.7	7.92
0.25 N_2	7.7	7.6
0.3 O_2	9.03	7.52
0.3 N_2	9.03	8.6

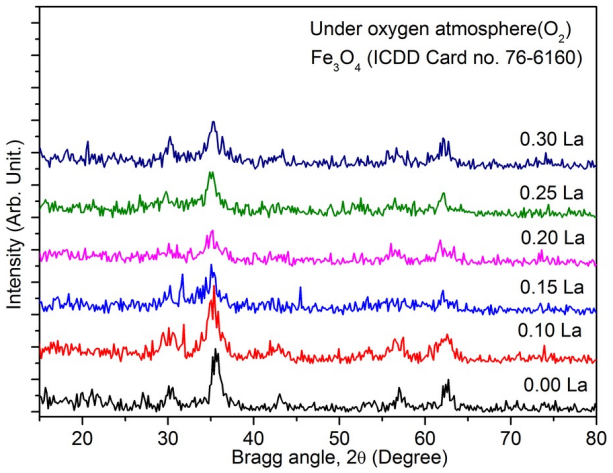

Figure 3: XRD patterns of co-doped Zn^{2+} and La^{3+} ions Fe_3O_4 nanopowders doped with different La^{3+} ion molar ratios synthesized via co-precipitation route under O_2 atmosphere at room temperature.

The UV-VIS-NIR absorption spectrum was recorded by a double-beam UV-VIS-NIR spectrophotometer. Diffuse reflectance measurements were done on the Jasco-V-570 spectrophotometer (Japan) fitted with integrating sphere reflectance unit.

The magnetic properties were accomplished of produced hexagonal ferrite samples at room temperature using a 7400-1 VSM (Lake Shore Cryotronics, Ltd, USA) in a maximum applied field of 20 kOe. From the obtained hysteresis behavior, the saturation magnetization (M_s), remanence magnetization (M_r), and coercivity (H_c) were determined.

3. Results and discussion

3.1. XRD analysis

Figures 3 and 4 demonstrate the XRD patterns for samples of pure magnetite (Fe_3O_4) and the Zn^{2+} and La^{3+} ions co-doped magnetite nanostructures for content $x = (0.0, 0.10, 0.15, 0.20, 0.25, \text{and } 0.30)$ at room temperature,

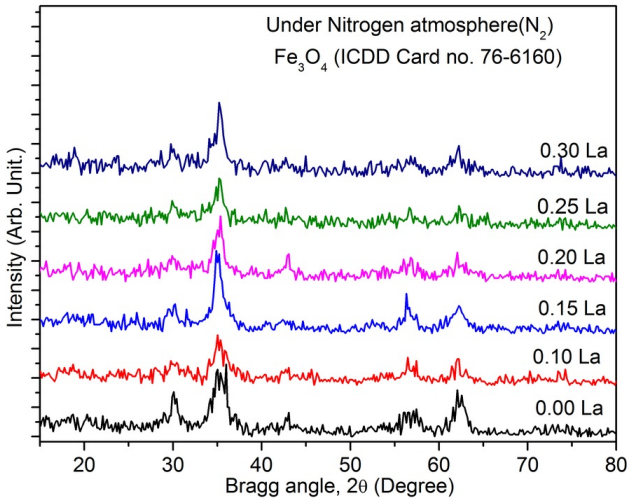

Figure 4: XRD patterns of co-doped Zn^{2+} and La^{3+} ions Fe_3O_4 nanopowders doped with different La^{3+} ion molar ratios synthesized via co-precipitation route under N_2 atmosphere at room temperature.

respectively. The XRD peaks for all (1-x)Fe_3O_4:Zn:xLa display that all peaks corresponded to those of magnetite (Fe_3O_4) cubic structure for space group *Fdm3* correlated to the standard JCPDS card #75-1610 file which shows that all of the observed diffraction peaks (220), (222), (400), (442), (511), and (440), at $2\theta = 30$, 35.5, 43, 53.5, 57, and 62.2, respectively. The other XRD patterns of N_2 atmosphere La^{3+} ion-doped at x from 0.00 and 0.30 molar ratio exhibit crystal phase of magnetite (Fe_3O_4) cubic structure referenced to the standard JCPDS card #75-1610 file without any secondary phases as shown in Figure 4.

It can be concluded, obviously, that the La^{3+} ion-doped led to a decrease in the crystallite size of the cubic magnetite (Fe_3O_4) phase. The crystallite size of Zn^{2+} and La^{3+} ions co-doped F_3O_4 nanopowders was estimated from the most intense peak (3 1 1) from XRD data based on Debye-Scherrer formula. However, at the nitrogen atmosphere, the crystallite size of cubic magnetite (Fe_3O_4) was 8.0 nm, which was smaller than at the oxygen atmosphere (9.8 nm). The crystallite size was found to be decreasing from 9.8 nm to 6.6 nm for the increasing La^{3+} doping from as low dopant concentration as 0.00 to as high as 0.30 molar ratio, respectively as well as crystallite size using nitrogen atmosphere decreasing from 8.0 nm to 3.9 nm as listed in Tables 5 and 6.

The lattice parameter of the samples was calculated using the following equation:

$$d_{hkl} = \frac{a}{\sqrt{h^2 + k^2 + l^2}}, \tag{2}$$

where a is the lattice parameter, d is the inter-planar distance, and h, k, and l are the Miller indices. The values of the lattice parameter were listed in Tables 5 and 6. The lattice parameter was increased with mounting La content of (1-x)Fe_3O_4:Zn:xLa nanoparticles because of a higher ionic radius of La^{3+} ions (2.74 Å) in comparison to the Fe^{3+} ions (1.72 Å) [18]. It was found that the volume of the unit cell increases with increasing La content which may be due to increasing the lattice parameter and values of the volume of the unit cell are tabulated in Tables 5 and 6. The X-ray theoretical density was estimated using the equation

$$\rho_x = \frac{\sum A}{N_A V}, \tag{3}$$

where ρ_x is the X-ray theoretical density, A is the sum of the atomic weights of all the atoms in the unit cell, V is the volume of the unit cell, and N_A is the Avogadro's number [19]. The X-ray theoretical density diminishes with rising La content of (1-x)Fe_3O_4:Zn:xLa nanoparticles. It may be due to the increasing volume of the unit cells as well as the increasing molecular weight of the product samples. The molecular weight of La (138.91 amu) ions and the ionic radii 2.74 Å are higher than that of Fe (55.85 amu) ions with ionic radii 1.72 Å. The values of the X-ray density of Zn^{2+} and La^{3+} ions co-doped magnetite nanoparticles were listed in Tables 5 and 6.

3.2. Microstructure

3.2.1. SEM analysis

Figures 5 and 6 show SEM and HR-TEM of Zn^{2+} and La^{3+} ions co-doped magnetite (Fe_3O_4) nanopowders for content $x = (0.0, 0.2,$ and 0.3 molar ratios) via co-precipitation route under O_2 and N_2 atmosphere at room temperature. Fine-scale Zn^{2+} and La^{3+} ions co-doped magnetite (Fe_3O_4) microstructure considers two frustrating problems arising for quantifying the microstructure. First, due to the small Zn^{2+} and La^{3+} ions co-doped magnetite grains less than 16 mm for the O_2 atmosphere and 12.0 nm for the N_2 atmosphere, manual measurements may need to be performed at magnifications 150.000×. Second, the fine magnetite with an appearance of island locates along magnetite grain boundaries or at triple junctions.

3.2.2. HR-TEM analysis

FE-SEM images in Figures 5 and 6 do not allow us to see the microstructures of Zn^{2+} and La^{3+} ions co-doped magnetite (Fe_3O_4) nanoparticles. The HR-TEM analysis will be useful for these two frustrating problems that arise for quantifying the microstructure. For the O_2 atmosphere, the majority of the particles present cubic morphology, characteristic of magnetite, as well as in the N_2 atmosphere the particles present the pseudocubic-shaped morphology, also characteristic of magnetite. The irregular geometry of Zn^{2+} and La^{3+} ions co-doped magnetite (Fe_3O_4) nanoparticles O_2 and N_2 atmosphere nanoparticles reflects their low crystallinity

Table 5: Variation of crystallite size lattice parameters cell volume, X-ray density, and bandgap energy of co-doped Zn^{2+} and La^{3+} ions Fe_3O_4 nanopowders doped with different La^{3+} ion molar ratios and synthesized via co-precipitation route under O_2 atmosphere at room temperature.

La^{3+} ions molar ratios	Formed phase	Crystallite size, D_x (nm)	Lattice constant, a (Å)	Unit cell volume, V (Å^3)	X-ray density, d_x (g/cm^3)	Optical bandgap energy (eV)
0.00	Fe_3O_4	9.0	8.358	583.801	8.756	1.80
0.10		7.1	8.382	588.987	9.2513	1.98
0.15		3.9	8.465	606.646	9.2600	1.92
0.20		7.3	8.432	599.558	9.651	1.87
0.25		6.0	8.466	606.696	9.8153	2.02
0.30		6.5	8.401	592.918	10.328	1.95

Table 6: Variation of crystallite size lattice parameters cell volume, X-ray density, and bandgap energy of co-doped Zn^{2+} and La^{3+} ions Fe_3O_4 nanopowders doped with different La^{3+} ion molar ratios and synthesized via co-precipitation route under N_2 atmosphere at room temperature.

La^{3+} ions molar ratios	Formed phase	Crystallite size, D_x (nm)	Lattice constant, a (Å)	Unit cell volume, V (Å^3)	X-ray density, d_x (g/cm^3)	Optical bandgap energy (eV)
0.00	Fe_3O_4	6.6	8.453	603.912	8.464	1.75
0.10		7.0	8.440	601.250	9.063	1.83
0.15		8.0	8.484	610.569	9.201	1.88
0.20		8.0	8.449	603.109	9.594	1.91
0.25		6.7	8.430	599.133	9.939	1.97
0.30		6.6	8.423	597.685	10.246	2.02

showed by XRD results. Therefore, the chemical precipitation of Zn^{2+} and La^{3+} ions co-doped and mixed Fe^{2+}/Fe^{3+} solution allowed to obtain particles with diameters significantly smaller than the chemical precipitation of only Fe^{2+} solution. The decrease in diameter can be directly related to higher surface areas and more reactive systems of Zn^{2+} and La^{3+} ions co-doped Fe_3O_4 nanoparticles.

FE-SEM revealed that at the oxygen atmosphere, La ions led to the formation of aggregates that are polydispersed and have many shapes as plates and rods as shown in Figure 5(c). When La ions increased, cracks were formed as shown in Figure 5(e), that is due to the separation of La ions from the magnetite nanoparticles, and also it led to a decrease of magnetism. HR-TEM clarified accurately the separation of La ions Figure 5(f). In the case of nitrogen, magnetite has very tiny particles and high dispersity as shown in Figures 6(a) and 6(b) which have no La ions, but when La ions were added, aggregates were formed in the shape of rods as shown in Figures 6(c) and 6(d). The increase of La ions led to the formation of conglomerates papers which appear in SEM as shown in Figure 6(e), but appear objectively in HR-TEM as separated rods due to separation of La ions from magnetite as shown in Figure 6(f).

3.3. Optical properties (UV-Vis-NIR spectroscopy characteristics)

The optical properties measurements were taken over the wavelength range 200–1,200 nm using integrating sphere unit of the spectrophotometer. Optical absorbance and diffuse reflectance spectra of Zn^{2+} and La^{3+} ions co-doped magnetite (Fe_3O_4) nanopowders via co-precipitation route under O_2 and N_2 atmosphere at room temperature curves are shown in Figures 7 and 8.

Apparently, the optical reflectance of the nanopowders was highly dependent on La^{3+} ions content and under O_2 and N_2 atmosphere route as shown in Figures 7 and 8. However, the absorbance spectra for the O_2 atmosphere in the IR region were smaller than the N_2 atmosphere absorbance spectra. The as-deposited sample exhibited the highest optical reflectivity of around 12–14% and 10–13% for O_2 and N_2 atmosphere, respectively, in the infrared (IR) and visible regions. Further increasing in La^{3+} ions doping was found to change the average reflectivity of around 45–28% in the IR and visible regions, respectively.

There was a definite drop in reflectance as the La^{3+} ions doped increased. Furthermore, the results revealed that the recorded absorbance was a characteristic peak of Fe and La ions.

In the limiting case of an infinite powder sample, thickness and sample holders have no influence on the value of reflectance (R). In this case, the Kubelka-Munk equation at any wavelength becomes

$$F(R\infty) = (100 - R)/(2R), \tag{4}$$

where $F(R\infty)$ is the so-called remission or Kubelka-Munk function. In the parabolic band structure, the bandgap Eg,

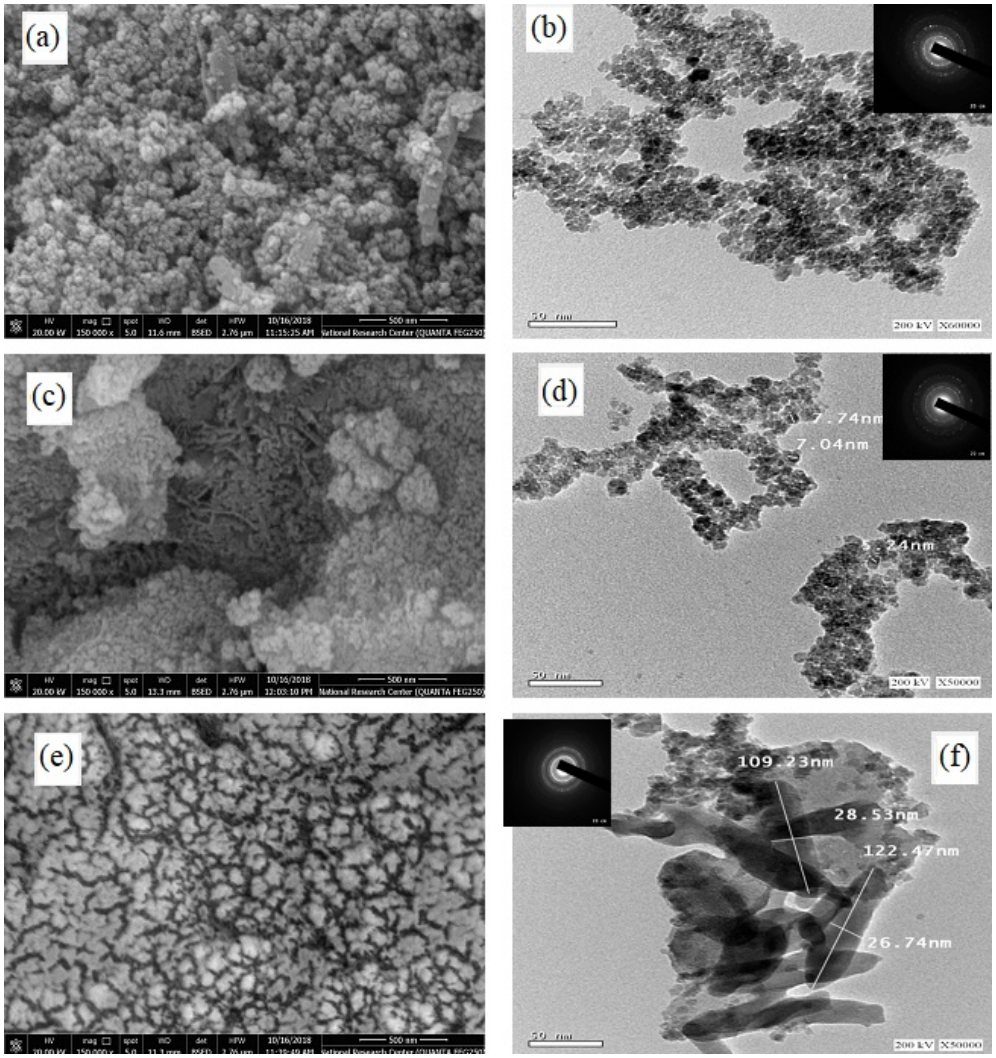

Figure 5: FE-SEM and HR-TEM of co-doped Zn^{2+} and La^{3+} ions Fe_3O_4 nanopowders doped with different La^{3+} ion molar ratios: (a-b) 0.0 La^{3+} ion, (c-d) 0.2 La^{3+} ion, and (e-f) 0.3 La^{3+} ion, synthesized via co-precipitation route under O_2 atmosphere at room temperature.

and absorption coefficient α, of a direct bandgap semiconductor are related through the well-known equation

$$\alpha h\nu = A(h\nu - Eg)^{1/n}, \tag{5}$$

where α is the linear absorption coefficient of the material, $h\nu$ is the photon energy, and A is proportionality constant. When the material scatters in a perfectly diffuse manner (or when it is illuminated at 60± incidence), the K-M absorption coefficient K becomes equal to 2α ($K = 2\alpha$). In this case, considering the K-M scattering coefficient S as constant with respect to wavelength, and using the remission function in (6) we obtain the expression

$$\big(h\nu F(R\infty)\big)^n = B(h\nu - Eg). \tag{6}$$

Therefore, obtaining $F(R\infty)$ from (6) and plotting the $[F(R\infty)h\nu]^2$ against $h\nu$, the bandgap Eg of a powder sample can be extracted easily. The bandgap energy of Zn^{2+} and La^{3+} doped Fe_3O_4 nanoparticles with different La^{3+} ion molar ratio after Kubelka-Munk treatment was shown in Figures 9 and 10. The direct bandgap energy of 0.0 La ion molar ratio sample was 1.80 eV for the O_2 atmosphere and 1.75 eV for the N_2 atmosphere. However, direct bandgap energy of Zn^{2+} and La^{3+} ions co-doped magnetite (Fe_3O_4) nanoparticles have rising values as the La^{3+} concentration increased from 0.0 to 0.3 molar ratios to bandgap energy of 2.02 eV in both O_2 and N_2 atmosphere and these values are summarized and listed in Tables 5 and 6.

3.4. Magnetic properties

The magnetization of the produced (1-x)Fe_3O_4:Zn:xLa was prepared via co-precipitation method under an applied field of 20 kOe and the hysteresis loops were

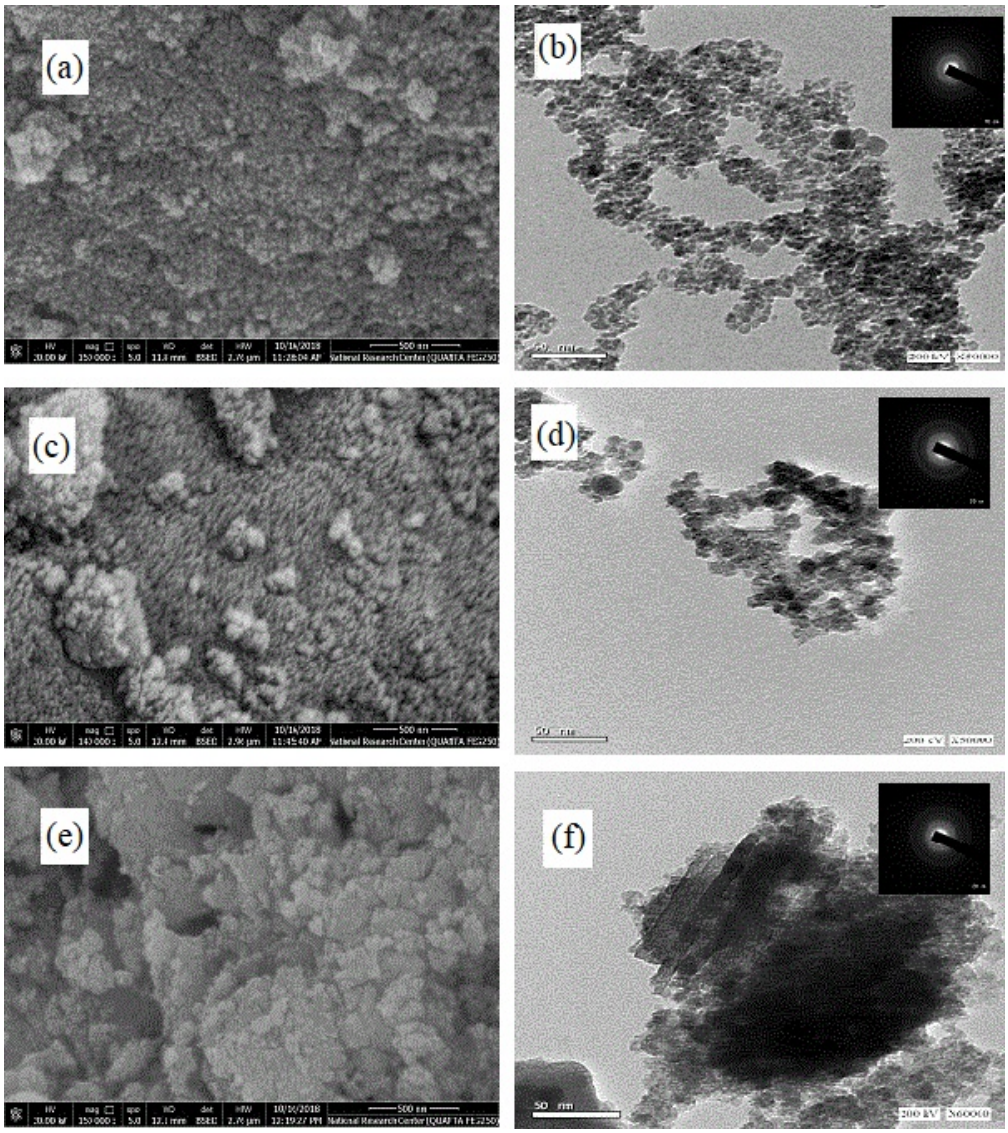

Figure 6: FE-SEM and HR-TEM of co-doped Zn^{2+} and La^{3+} ions Fe_3O_4 nanopowders doped with different La^{3+} ion molar ratios: (a-b) 0.0 La^{3+} ion, (c-d) 0.2 La^{3+} ion, and (e-f) 0.3 La^{3+} ion, synthesized via co-precipitation route under N_2 atmosphere at room temperature.

determined. Plots of magnetization (M) as a function of the magnetic field (H) for different La^{3+} and Sm^{3+} molar ratios at room temperature under oxygen and nitrogen atmosphere are shown in Figures 11 and 12. The saturation magnetization and remanence magnetization with oxygen atmosphere [$M_s = 32.872$ emu/g and $M_r = 0.078$ emu/g] were decreasing with changing atmosphere to nitrogen gas [$M_s = 24.789$ emu/g and $M_r = 0.0482$ emu/g]. However, the coercivity was increasing with a changing atmosphere from oxygen to nitrogen gas from $H_c = 3.837$ Oe to $H_c = 7.946$ Oe, respectively, belonging to phase formation, degree of crystallinity, crystallite size, and microstructure. The results can be explained on the basis of decreasing phase formation, degree of crystallinity, crystallite size, and microstructure. From the obtained hysteresis loops, the saturation magnetization (M_s), remanence magnetization (M_r), and coercivity (H_c) are listed in Tables 7 and 8. Room temperature magnetization measurements showed that there is a decrease in the saturation magnetization (M_s), with increasing the La^{3+} molar ratios from 0.1 to 0.3, from 18.813 emu/g to 3.915 emu/g, respectively in oxygen atmosphere. Meanwhile, in nitrogen atmosphere saturation magnetization (M_s) was decreasing from 16.723 emu/g to 3.623 emu/g with increasing the La molar ratios from 0.1 to 0.3, respectively. Furthermore, increasing the doping Zn^{2+} and La^{3+} ions does not allow the atomic diffusion into each particle to change its chemical homogeneity and induced partial densification affecting the strength

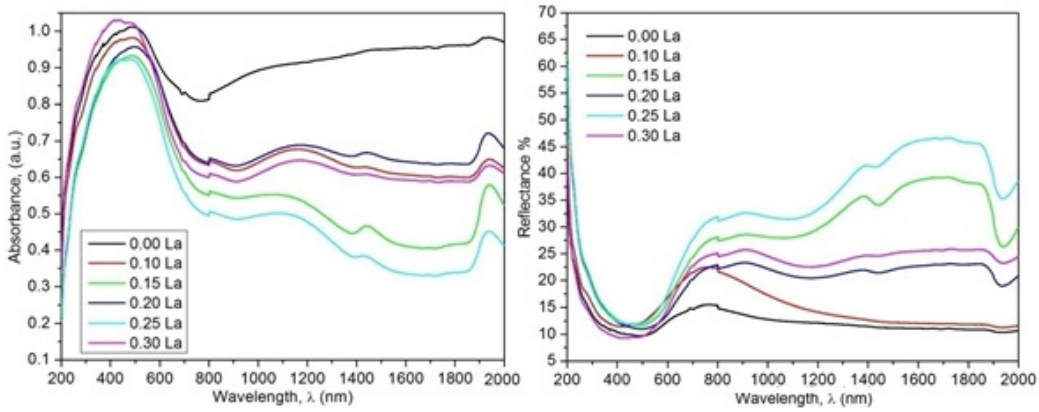

Figure 7: Optical absorbance and diffuse reflectance spectra of co-doped Zn^{2+} and La^{3+} ions Fe_3O_4 nanopowders, doped with different La^{3+} ion molar ratios and synthesized via co-precipitation route under O_2 atmosphere at room temperature.

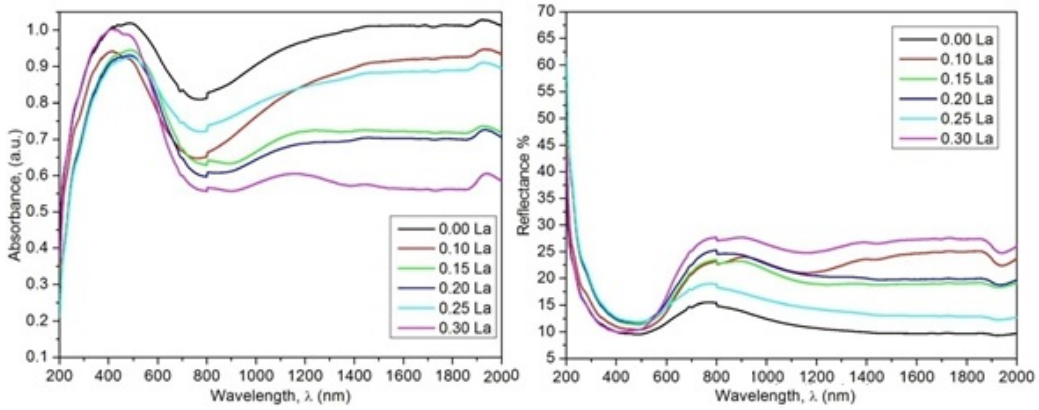

Figure 8: Optical absorbance and diffuse reflectance spectra of co-doped Zn^{2+} and La^{3+} ions Fe_3O_4 nanopowders, doped with different La^{3+} ion molar ratios and synthesized via co-precipitation route under N_2 atmosphere at room temperature.

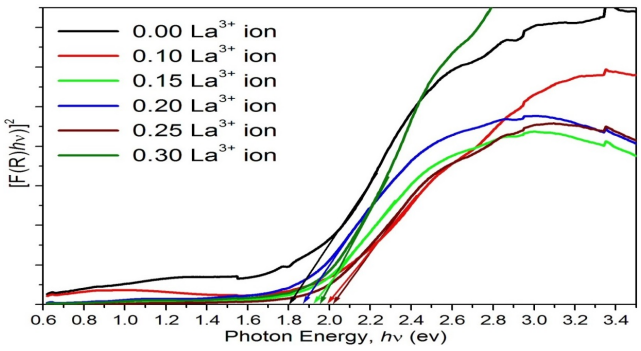

Figure 9: Optical bandgap of co-doped Zn^{2+} and La^{3+} ions Fe_3O_4 nanopowders, doped with different La^{3+} ion molar ratios and synthesized via co-precipitation route under O_2 atmosphere at room temperature.

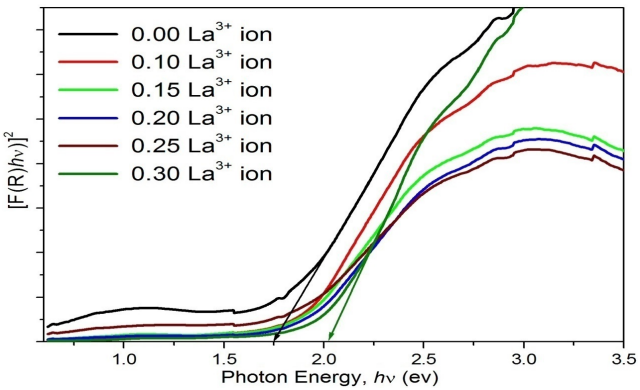

Figure 10: Optical bandgap of co-doped Zn^{2+} and La^{3+} ions Fe_3O_4 nanopowders, doped with different La^{3+} ion molar ratios and synthesized via co-precipitation route under N_2 atmosphere at room temperature.

of dipolar interactions. The decrease in magnetization is also expected after substitution since La^{3+} ions have a lower magnetic moment of $0\,\mu_B$ whereas Fe^{3+} ion is $5\,\mu_B$, which enhanced inter-sub-lattice A−B super-exchange interaction between the magnetic ions of the sub-lattices,

Table 7: The magnetic properties on co-doped Zn^{2+} and La^{3+} ions Fe_3O_4 nanopowders doped with different La^{3+} ion molar ratios synthesized via co-precipitation route under O_2 atmosphere at room temperature.

La^{3+} ions molar ratios	Magnetic properties				
	Saturation magnetization M_s, (emu/g)	**Retentivity M_r, ($\times 10^{-3}$ emu/g)**	**Coercivity H_c, (Oe)**	**Remanence ratio, $\times 10^{-6}$ M_r/M_s**	**Magnetic moment per mole μ_B**
0.00	32.872	78.459	3.8379	2.387	2.265
0.10	18.813	126.55	8.216	6.727	1.382
0.15	8.609	9.717	12.559	1.129	0.652
0.20	4.542	11.906	16.633	2.622	0.354
0.25	4.342	9.096	20.829	2.095	0.349
0.30	3.916	7.991	24.916	2.041	0.323

Table 8: The magnetic properties on co-doped Zn^{2+} and La^{3+} ions Fe_3O_4 nano powders doped with different La^{3+} ion molar ratios synthesized via co-precipitation route under N_2 atmosphere at room temperature.

La^{3+} ions molar ratios	Magnetic properties				
	Saturation magnetization M_s, (emu/g)	**Retentivity M_r, ($\times 10^{-3}$ emu/g)**	**Coercivity H_c, (Oe)**	**Remanence ratio, $\times 10^{-6}$ M_r/M_s**	**Magnetic moment per mole μ_B**
0.00	24.789	48.224	7.946	1.945	1.708
0.10	16.723	21.167	8.012	1.266	1.228
0.15	14.645	33.269	10.74	2.272	1.109
0.20	15.630	22.790	4.206	1.458093	1.219
0.25	16.167	688.88	67.032	42.610255	1.298
0.30	3.623	72.241	112.260	19.938452	0.299

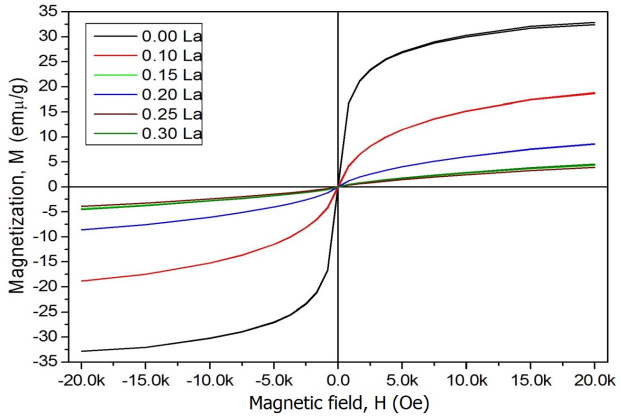

Figure 11: M-H loops of co-doped Zn^{2+} and La^{3+} ions Fe_3O_4 nanopowders doped with different La^{3+} ion molar ratios synthesized via co-precipitation route under O_2 atmosphere at room temperature.

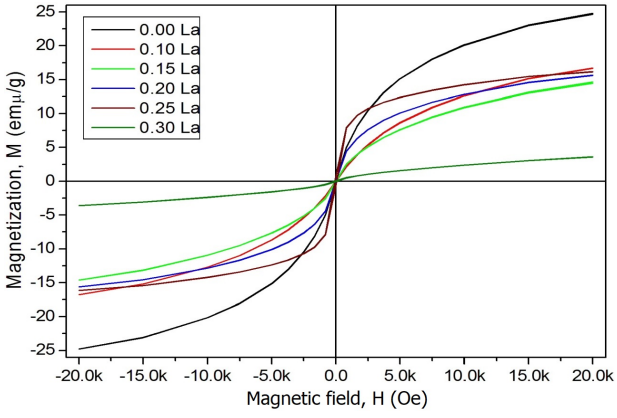

Figure 12: M-H loops of co-doped Zn^{2+} and La^{3+} ions Fe_3O_4 nano powders doped with different La^{3+} ion molar ratios synthesized via co-precipitation route under N_2 atmosphere at room temperature.

A and B. Surface effects were led to a formation of a magnetic dead layer resulting in a decrease in M_s. With increasing magnetic Zn^{2+} and La^{3+} concentration (x), the super-exchange interactions among A−O−B in the system have been strengthened. The net magnetic moment of the whole lattice is the difference between the A- and B-sublattices, that is, M = MB − MA, where MA and MB are the magnetization of the A and B sites, respectively. Therefore, the decrease in M_s and M_r can be attributed to change of the super-exchange interactions among A−O−B.

The magnetic moment per molecule (μ_B) was obtained as summarized in Tables 7 and 8 using the empirical formula

$$\mu_B = \frac{M_{wt} \cdot M_s}{5585}, \tag{7}$$

where M_{wt} is molecular weight, M_s is saturation magnetization, and 5585 is a magnetic factor. It is observed that as La^{3+} content increases the μ_B values go to decrease. This might be attributed to that La^{3+} ions occupied the A-site and Fe^{3+} ions B-site and consequently resulting in an increase

of magnetic moment of B-site as well as an increase in the value of the magnetic moment of A-site. Low squareness ratio (M_r/M_s) and coercivity (H_c) values reflect the superparamagnetic nature of samples at different La^{3+} values. As a result, the M_r/M_s ratio for interacting superparamagnetic particles is approximately 0.10, that is, the sample loses its magnetization when the applied magnetic field is removed. As mentioned in Tables 7 and 8, all of the samples possessed a M_r/M_s ratio of less than 0.10.

4. Conclusion

Different techniques were used to ensure the phase in the nanocomposites and to confirm the formation of a single-phase structure. The stoichiometric ratios of the elements in the general formula of and to (1-x)Fe_3O_4:Zn:xLa were proved and confirmed by EDX, ICP, and atomic absorption data. Characterization techniques have been used to analyze and characterize the prepared nanoparticles. XRD confirms the formation of one single phase of nanoparticles components with average crystalline size ranging from 6.0 nm to 9.0 nm at oxygen atmosphere and 6.0 nm to 8.0 nm at the nitrogen atmosphere. The morphology of Zn^{2+} and La^{3+} ions co-doped magnetite nanoparticles was studied using FE-SEM and HR-TEM. Optical properties were demonstrated by UV-visible-NIR spectrophotometer. Magnetic properties of the given samples were obtained from VSM.

Conflict of interest The authors declare that they have no conflict of interest.

References

[1] S. Saqib, M. F. H. Munis, W. Zaman, F. Ullah, S. N. Shah, A. Ayaz, et al., *Synthesis, characterization and use of iron oxide nano particles for antibacterial activity*, Microsc Res Tech, 82 (2019), 415–420.

[2] W. Wu, Z. Wu, T. Yu, C. Jiang, and W. S. Kim, *Recent progress on magnetic iron oxide nanoparticles: synthesis, surface functional strategies and biomedical applications*, Sci Technol Adv Mater, 16 (2015), 023501.

[3] L. Yang, Z. Cao, H. K. Sajja, H. Mao, L. Wang, H. Geng, et al., *Development of receptor targeted magnetic iron oxide nanoparticles for efficient drug delivery and tumor imaging*, J Biomed Nanotechnol, 4 (2008), 439–449.

[4] S. Laurent, S. Dutz, U. O. Hafeli, and M. Mahmoudi, *Magnetic fluid hyperthermia: focus on superparamagnetic iron oxide nanoparticles*, Adv Colloid Interface Sci, 166 (2011), 8–23.

[5] A. H. Lu, E. L. Salabas, and F. Schuth, *Magnetic nanoparticles: synthesis, protection, functionalization, and application*, Angew Chem Int Ed Engl, 46 (2007), 1222–1244.

[6] X. H. Peng, X. Qian, H. Mao, A. Y. Wang, Z. G. Chen, N. S., et al., *Targeted magnetic iron oxide nanoparticles for tumor imaging and therapy*, Int J Nanomedicine, 3 (2008), 311–321.

[7] W. Wu, X. Xiao, S. Zhang, J. Zhou, L. Fan, F. Ren, et al., *Large-scale and controlled synthesis of iron oxide magnetic short nanotubes: shape evolution, growth mechanism, and magnetic properties*, J Phys Chem C Nanomater Interfaces, 114 (2010), 16092–16103.

[8] G. Martínez, A. Malumbres, R. Mallada, J. L. Hueso, S. Irusta, O. Bomatí-Miguel, et al., *Use of a polyol liquid collection medium to obtain ultrasmall magnetic nanoparticles by laser pyrolysis*, Nanotechnology, 23 (2012), 425605.

[9] C. Boxall, G. Kelsall, and Z. Zhang, *Photoelectrophoresis of colloidal iron oxides. Part 2.—Magnetite (Fe_3O_4)*, J Chem Soc Faraday Trans, 92 (1996), 791–802.

[10] K. Srinivasa Rao, S. V. Ranga Nayakulu, M. Chaitanya Varma, G. S. V. R. K. Choudary, and K. H. Rao, *Controlled phase evolution and the occurrence of single domain $CoFe_2O_4$ nanoparticles synthesized by PVA assisted sol-gel method*, J Magn Magn Mater, 451 (2018), 602–608.

[11] E. M. M. Ibrahima, L. H. Abdel-Rahman, A. M. Abu-Dief, A. Elshafaie, S. K. Hamdan, and A. M. Ahmed, *Electric, thermoelectric and magnetic characterization of γ-Fe_2O_3 and Co_3O_4 nanoparticles synthesized by facile thermal decomposition of metal-Schiff base complexes*, Mater Res Bull, 99 (2018), 103–108.

[12] L. B. de Mello, L. C. Varanda, F. A. Sigoli, and I. O. Mazali, *Co-precipitation synthesis of (Zn-Mn)-co-doped magnetite nanoparticles and their application in magnetic hyperthermia*, J Alloys Compd, 779 (2019), 698–705.

[13] R. Abazari, A. R. Mahjoub, S. Molaie, F. Ghaffarifar, E. Ghasemi, A. M. Z. Slawin, et al., *The effect of different parameters under ultrasound irradiation for synthesis of new nanostructured Fe_3O_4@bio-MOF as an efficient anti-leishmanial in vitro and in vivo conditions*, Ultrason Sonochem, 43 (2018), 248–261.

[14] A. M. Mazrouaa, M. G. Mohamed, and M. Fekry, *Physical and magnetic properties of iron oxide nanoparticles with a different molar ratio of ferrous and ferric*, Egypt J Pet, 28 (2019), 165–171.

[15] C. C. Berry and A. S. G. Curtis, *Functionalisation of magnetic nanoparticles for applications in biomedicine*, J Phys D Appl Phys, 36 (2003), R198–R206.

[16] L. Pranita and J. Preeti, *Preparation and characterization of zinc doped magnetite nanoparticles using green synthesis*, Int J Res Chem Environ, 5 (2015), 60–64.

[17] U. Holzwarth and N. Gibson, *The scherrer equation versus the 'Debye-Scherrer equation'*, Nat Nanotechnol, 6 (2011), 534.

[18] D. E. Hogan, *Biosurfactant (monorhamnolipid) complexation of metals and applications for aqueous metalliferous waste remediation*, PhD thesis, The University of Arizona, 2016.

[19] R. F. Fox, T. P. Hill, and R. M. Fox, *Macroscope: An exact value for Avogadro's number*, Am Sci, 95 (2007), 104–107.